Polyhedron 111 (2016) 64–70

Contents lists available at ScienceDirect

Polyhedron

journal homepage: www.elsevier.com/locate/poly

Tuning the photophysical properties of a (*P,N*)Re^{I} complex by adding a –NH– fragment into a *P,N*-bidentate ligand: The case of [*P,N*-{$(C_6H_5)_2(C_5H_4N)NHP$}$Re(CO)_3Br$]

Pablo Mella [a], Juan Carlos Palma [a], Marjorie Cepeda-Plaza [a], Pedro Aguirre [b], Jorge Manzur [c,e], Germán Günther [d], Nancy Pizarro [a], Andrés Vega [a,e,*]

[a] Universidad Andres Bello, Facultad de Ciencias Exactas, Departamento de Ciencias Químicas, Chile
[b] Universidad de Chile, Facultad de Ciencias Químicas y Farmacéuticas, Departamento de Química Analítica e Inorgánica, Chile
[c] Universidad de Chile, Facultad de Ciencias Físicas y Matemáticas, Departamento de Ciencia de Los Materiales, Chile
[d] Universidad de Chile, Facultad de Ciencias Químicas y Farmacéuticas, Departamento de Química Orgánica y Fisicoquímica, Chile
[e] Centro para el Desarrollo de la Nanociencia y la Nanotecnología, CEDENNA, Chile

ARTICLE INFO

Article history:
Received 23 December 2015
Accepted 8 March 2016
Available online 18 March 2016

Keywords:
(*P,N*,N)Re^{I}-tricarbonyl complex
Biexponential emission lifetime
Intra-Ligand
Luminescence
NH-fragment

ABSTRACT

The spectroscopic, electrochemical and photophysical properties of the new complex [*P,N*-{$(C_6H_5)_2(C_5H_4N)NHP$}$Re(CO)_3Br$] (**RePNN**) are reported. The UV–Vis spectrum in dichloromethane (DCM) shows an absorption maximum centered at 300 nm and a shoulder at 350 nm. These absorption bands have been characterized, having a $\pi_{py} \rightarrow \pi^*_{py}$ and a MLCT character. Excitation at the first wavelength (higher energy) leads to an emission band centered at 365 nm. Cyclic voltammetry shows a fully irreversible oxidation wave around +1.45 V, assigned to Re^{I}/Re^{II} couple, whereas two irreversible reduction signals centered at −0.75 and −1.20 V are assigned to ligand reduction processes. The photophysical results show that emission from the **RePNN** complex comes exclusively from the ligand. The MLCT excited state shows to be non-emissive by coupling to vibrational modes leading to non-radiative decay path to ground state. The luminescent decay fits to a bi-exponential function. DFT calculations suggest that intra-ligand $\pi_{py} \rightarrow \pi^*_{py}$ and $\pi_{py} \rightarrow \pi^*_{ph}$ excited states may account for the existence of these two decay lifetimes. The additional –NH– fragment present in the 2-(diphenylphosphinoamino)pyridine ligand compared to 2-pyridylphosphine, makes it more flexible and in consequence, enhances the non-radiative decay rate constant from the ^{3}MLCT to the ground state in the **RePNN** complex compared to those of 2-pyridylphosphine, [*P,N*-{$(C_6H_5)_2(C_5H_4N)PRe(CO)_3Br$] (**RePN**).

1. Introduction

Mononuclear Re^{I} tri-carbonyl complexes having a chelating *P,N*-molecule have been less studied compared to the corresponding N,N-diimines, despite the fact that the presence of a phosphorous atom at the coordination sphere of the metal may confer different properties, due to its trans-effect [1–7]. Examples of reported complexes with such *P,N*-ligands are limited to the simplest molecule of this kind, 2-pyridyldiphenylphosphine, $(C_6H_5)_2(C_5H_4N)P$. Examples are [{$(C_6H_5)_3P$}{*P,N*-$(C_6H_5)_2(C_5H_4N)P$}$ReCl_2$] [8] [{*O,N*-$(C_6H_5)_3P$}{$(C_6H_5)_2(C_5H_4N)PO$}$ReCl_3$] [9] or [{$(C_6H_5)_3P$}{*P,N*-$(C_6H_5)_2(C_5H_4N)P$}$Re(NO)_{0.87}Br_{2.13}$] [10]. We have recently reported the synthesis and preliminary emission properties of a novel Re^{I} complex, [*P,N*-{$(C_6H_5)_2(C_5H_4N)P$}$Re(CO)_3Br$] (**RePN**) (Scheme 1 left) [11]. In contrast to N,N-diimine Re^{I} complexes, with high luminescent quantum yields (0.01–0.30) and emission lifetimes of a hundred nanoseconds [12,13], the **RePN** complex shows a low emission quantum yield (less than 0.001) and a biexponential emission decay with short luminescence lifetimes (in the order of few nanoseconds) [11,14]. We have established by means of experimental and TDDFT analysis that the dual emission observed in such complex can be attributed to the existence of two excited states related to the π^*-systems on the pyridine and phenyl rings [14]. Closely related to 2-pyridyldiphenylphosphine ligand, 2-(diphenylphosphinoamino)pyridine (**PNN**) (Scheme 1 center) is another bidentate *P,N*-chelating molecule which would be useful for preparing new Re^{I} carbonyl complexes, to study the effect of having a phosphorus atom coordinated to the metal.

* Corresponding author at: Universidad Andres Bello, Facultad de Ciencias Exactas, Departamento de Ciencias Químicas, Chile.
E-mail address: andresvega@unab.cl (A. Vega).

http://dx.doi.org/10.1016/j.poly.2016.03.014
0277-5387/

Scheme 1. [*P,N*-{$(C_6H_5)_2(C_5H_4N)P$}$Re(CO)_3Br$] (**RePN**) (left) 2-(diphenylphosphinoamino)pyridine (**PNN**) (center) and [*P,N*-{$(C_6H_5)_2(C_5H_4N)NHP$}$Re(CO)_3Br$] (**RePNN**) (right).

Recently Aranda et al. [15] have prepared an Ir^{III} derivative of **PNN**, showing a dramatic spectroscopic effect when a NH-fragment is inserted between the phosphorous and the pyridyl groups, which is reflected in a blue shift of the emission. In the present work, we describe the synthesis of the complex [*P,N*-{$(C_6H_5)_2(C_5H_4N)NHP$}$Re(CO)_3Br$] (**RePNN**) (Scheme 1 right), and its spectroscopic, electrochemical and photophysical properties. The experimental results were also analyzed according to DFT/TDDFT computational calculations. A comparison of this study with the previously informed for **RePN** is also presented.

2. Experimental

All reagents, $(Re(CO)_3(THF)Br)_2$ (THF:tetrahydrofuran) and 1,10-phenanthroline were used as received from the supplier (Aldrich), with no purification before use. Solvents were dried and freshly distilled before use. Standard Schlenk techniques were used for all manipulations. 2-(diphenylphosphinoamino)pyridine was prepared according a previously described method [15].

2.1. Synthesis

The **RePNN** complex was prepared following the previously reported method described for **RePN** synthesis [11].

Briefly, a solution of 331.0 mg of 2-(diphenylphosphinoamino) pyridine (**PNN**) (1.18 mmol) in chloroform (20 mL) was added to a solution of 501.7 mg of $[ReBr(CO)_3(C_4H_8O)]_2$ (0.592 mmol) in chloroform (20 mL), and stirred at room temperature during 24 h. Addition of cyclohexane precipitates the complex, allowing the isolation of 500 mg of crude (67.1% yield). Recrystallization by slow diffusion of toluene/cyclohexane (3/2) to a chloroform solution yields almost transparent amber crystals, suitable for X-rays analysis. *Elemental Analysis*: Calculated (experimental) for $C_{20}H_{15}BrPN_2O_3Re$: C, 38.23 (37.77); H, 2.41 (2.56); N, 4.46 (4.19). Elemental analysis was obtained from Centro de Análisis Pontificia Universidad Católica de Chile. *IR*: ν_{CO}: 2050, 1910, 1890 cm^{-1}.

2.2. Structure determination

The crystal structure of **RePNN** at 273 K was determined by X-ray diffraction, on a plate-shaped 0.134 mm × 0.314 mm × 0.332 mm slightly amber transparent crystal. Data collection was done on a SMART-APEX II CCD diffractometer system. Data was reduced using SAINT [16], while the structure was solved by direct methods, completed by Difference Fourier Synthesis and refined by least-squares using SHELXL [17]. Multi-scan absorption corrections were applied using SADABS [18]. The hydrogen atoms positions were calculated after each cycle of refinement with SHELXL using a riding model for each structure, with C—H distance of 0.95 Å. $U_{iso}(H)$ values were set equal to 1.2 U_{eq} of the parent carbon atom. The final structure shows that the ellipsoids corresponding to the chlorine atoms of chloroform are elongated mainly in the perpendicular of the carbon to chlorine bond, and more important in the direction of the rotation around the C_3 molecular axis of chloroform.

2.3. Cyclic voltammetry

Cyclic voltammograms at 50, 100, 300, 500 and 600 mV s^{-1} at room temperature were recorded in DCM solutions (1.0 mM) using tetrabutylammonium perchlorate (0.10 M) as electrolyte. A vitreous carbon electrode was used as working electrode, a platinum electrode as auxiliary electrode, and a saturated calomel electrode as reference electrode. Iron ferrocene was used as internal standard.

2.4. Spectroscopic and photophysical measurements

UV–Vis spectra were recorded on an Agilent 8453 Diode-Array spectrophotometer in the range of 250–700 nm in both aerated dichloromethane (DCM) or dimethylformamide (DMF) solutions. Emission spectra were measured in a Horiba Jobin-Yvon FluoroMax-4 spectrofluorometer in both solvents mentioned previously at room temperature or in ethanol–methanol glass (4:1, v/v) at 77 K. Luminescence lifetime measurements were carried out with the time correlated single photon counting technique using a PicoQuant Fluotime 200 fluorescence lifetime spectrometer. Experiments were made in DCM solutions either air-equilibrated or argon-saturated. Quantum yield were measured using procedures described in literature using Quinine Sulfate in 0.1 M H_2SO_4 as standard compound [19].

2.5. Computational details

All geometry optimizations were performed at the B3LYP/6-31 +G(d,p) level of theory using the Gaussian09 Rev C.01 package of programs (G09) [20], and started from geometry determined by means of X-ray diffraction. The LANL2DZ basis set was used only for Rhenium. Excited state calculations were performed within the time-dependent DFT methodology as implemented in G09. Solvent effects for simulating dichloromethane have been incorporated through the polarizable continuum model (PCM) using the integral equation formalism variant (IEFPCM) [21,22]. Absorption and emission spectra were simulated from the above calculations using the GaussSum 3.0 suite of freely available processing tools. A full width at half-maximum (FWHM) of the Gaussian curves corresponding to 3000 cm^{-1} was employed to convolute both spectra. Representations for molecular orbitals were generated using the G09 cubegen tool and have been visualized using VMD and Povray 3.6 programs [23,24].

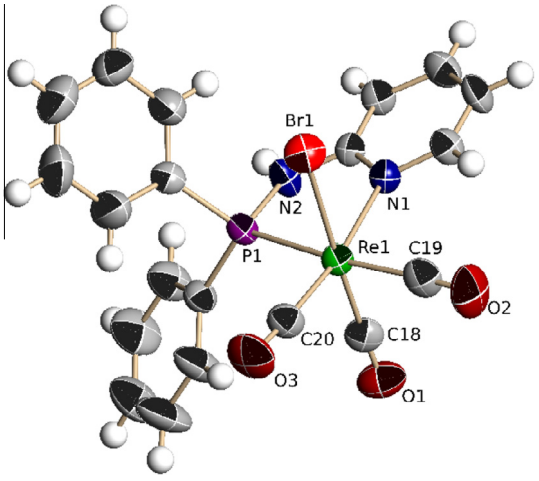

Fig. 1. Molecular structure diagram for **RePNN** showing atom numbering scheme. Displacement ellipsoids drawn at the 50% level of probability.

3. Results and discussion

3.1. Structural description

The structure of the **RePNN** complex can be described as a central Re^{I} ion octahedrally surrounded by three carbonyl groups (in a *fac* correlation), a bidentate **PNN** molecule and a bromide anion, as shown in Fig. 1.

Table 1
Selected bond distances (Å) and angles (°) for **RePNN**. Selected values corresponding to **RePN** [11] have been included between square brackets for comparison.

Re1—P1	2.4106(18) [2.5037(13)]	Re1—C18	1.914(9)
Re1—Br1	2.6125(9) [2.6187(6)]	Re1—C19	1.974(9)
Re1—N1	2.204(6) [2.201(4)]	Re1—C20	1.897(8)
C20—Re1—C18	91.6(3)	C19—Re1—N1	95.3(3)
C20—Re1—C19	89.9(3)	C20—Re1—P1	97.0(2)
C18—Re1—C19	88.5(4)	C18—Re1—P1	90.5(2)
C20—Re1—N1	171.4(3)	C19—Re1—P1	173.1(2)
C18—Re1—N1	95.4(3)	N1—Re1—P1	77.98(16) [64.9(1)]

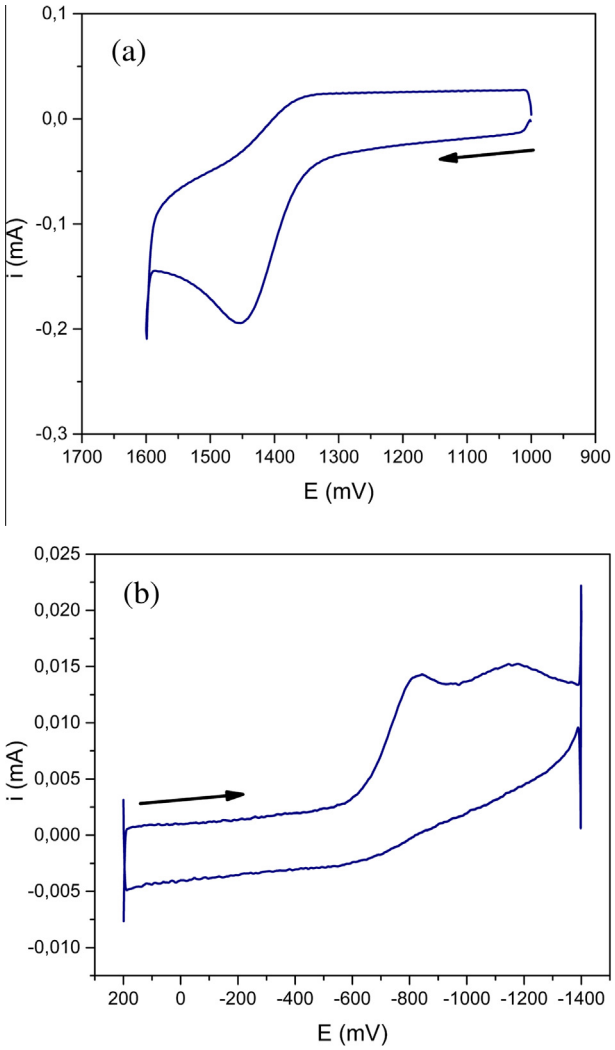

Fig. 2. Cyclic voltammogram of **RePNN**, measured in DCM containing $\{(C_4H_9)_4N\}^+ClO_4^-$ 0.10 M as supporting electrolyte with a glassy-carbon working electrode. (**a**) Oxidation wave. (**b**) Reduction wave. Arrows indicate the direction of the potential sweep.

In terms of molecular structure, **RePNN** has the same connectivity that **RePN**, except the –NH– moiety between the pyridyl group and the phosphorous atom in **PNN** compared to **PN**. As a consequence of that, the chelated ring is now five membered while for **RePN** is just four-membered. This is reflected mainly in the biting N-Re-P angle, 78.0(2)°, closer to the 90° expected for a regular octahedron than the value measured for **RePN**, 64.9(1)° (see Table 1).

3.2. Cyclic voltammetry

Cyclic voltammogram shows mainly two completely irreversible signals. A fully irreversible oxidation wave occurs at around +1.45 V, as shown in Fig. 2a. By comparison to **RePN** this process has been assigned to the metal-centered one-electron Re^{I}/Re^{II} couple.

Two fully irreversible reduction waves occur between −0.75 V and −1.20 V. By comparison to **RePN** and related compounds, the last of these bands has been assigned to a ligand reduction. In order to test this idea we have optimized the molecular structure of **RePNN** by means of DFT calculations. The computed structure in the gas phase closely resembles that determined by X-ray diffraction (Table S1). Vertical oxidation and reduction of the Re^{I} molecule leads to odd-electron species, where the unpaired electron mainly resides on the rhenium atom in the oxidized specie $\mathbf{RePNN}^{+}$ (Fig. 3a) and into the ligand in the reduced specie $\mathbf{RePNN}^{-}$ (Fig. 3b).

It is interesting to note that upon electron removal or addition, important distortions of the geometry of the corresponding species

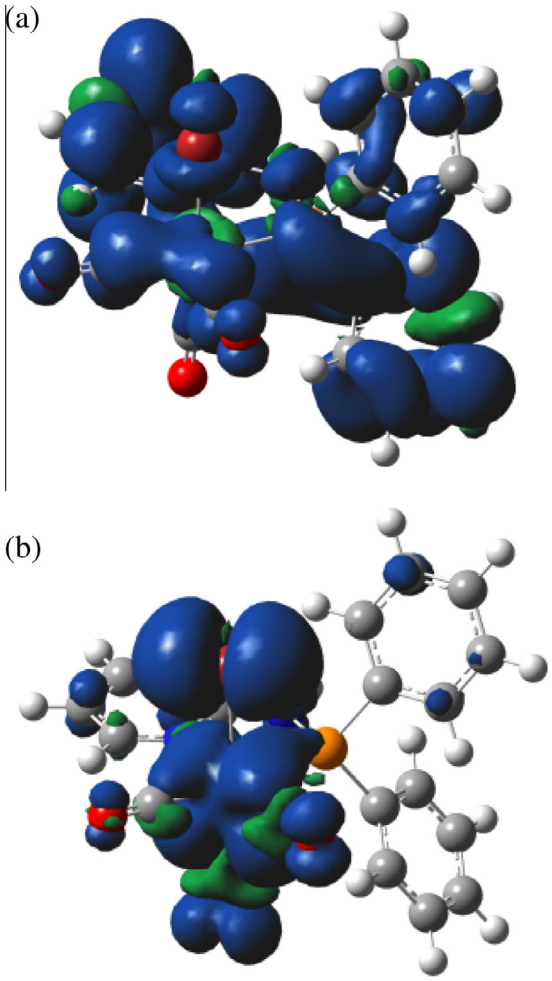

Fig. 3. Gas phase DFT computed spin density transitions for the vertical reduction (**a**) and oxidation (**b**) of **RePNN**.

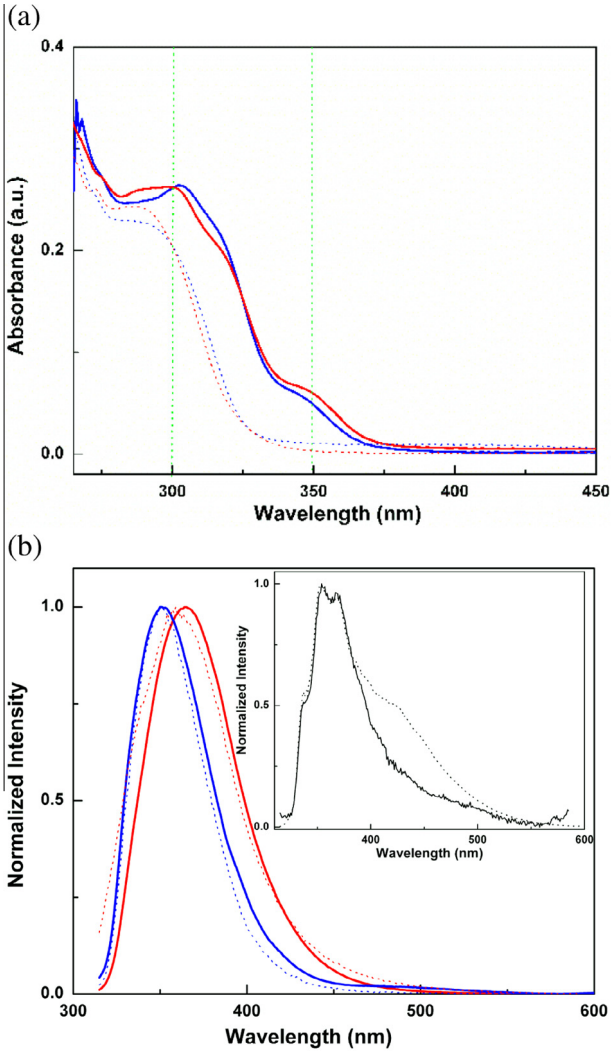

Fig. 4. (**a**) Absorption and (**b**) emission spectra of complex (solid lines) and ligand (dotted lines) in DCM (red) and DMF (blue) aerated solutions at room temperature. Emission spectra were recorded after excitation at 300 nm. ***Inset***: Emission spectra at 77 K of the complex in ethanol/methanol (4:1) after excitation at 300 nm (solid line). For comparison, ligand emission spectrum was included (dotted line). (**c**) Phosphorescence spectra of complex (solid line) and ligand (dotted line) in ethanol/methanol (4:1) at 77 K after delay of 50 μs and excitation at 300 nm. ***Inset***: Comparison of the phosphorescence intensity of complex and ligand. Spectra recorded in the same conditions (Color online.)

Table 2
Photophysical properties of the **RePNN** complex and the **PNN** ligand at room temperature.

	λ_{abs}, nm (ε, 10^3 M^{-1} cm^{-1})	λ_{em}, nm	Φ_{em}	τ_{em}, ns (%)
RePNN (Complex)				
DCM	300 (6.0); 350 (1.0)	365	0.013	6.37 (65); 2.26 (35)
DMF	300 (6.0); 350 (1.0)	350	0.011	7.23 (44); 3.60 (56)
PNN (Ligand)				
DCM	230 (19.0); 295 (4.5)	365	0.110	6.67 (3); 2.00 (97)
DMF	295 (4.5)	350	0.200	5.15

Values were no sensible to oxygen presence. Errors ± 10%.

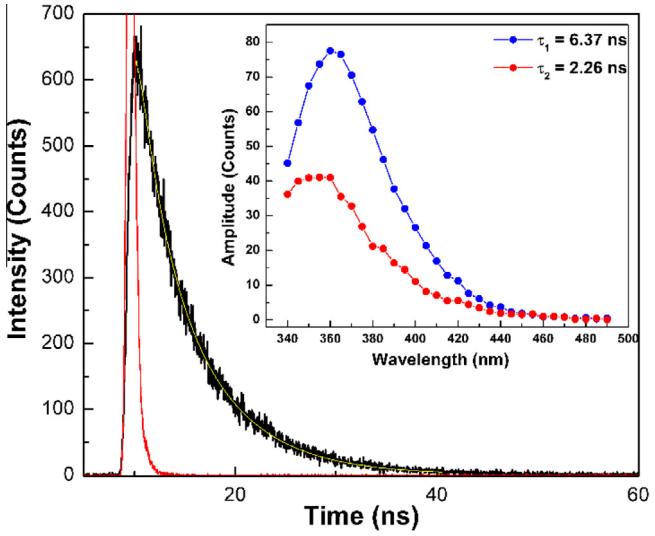

Fig. 5. Biexponential luminescent decay of the **RePNN** complex in DCM at 360 nm after excitation at 280 nm. ***Inset:*** Time-Resolved Emission Spectra (TRES).

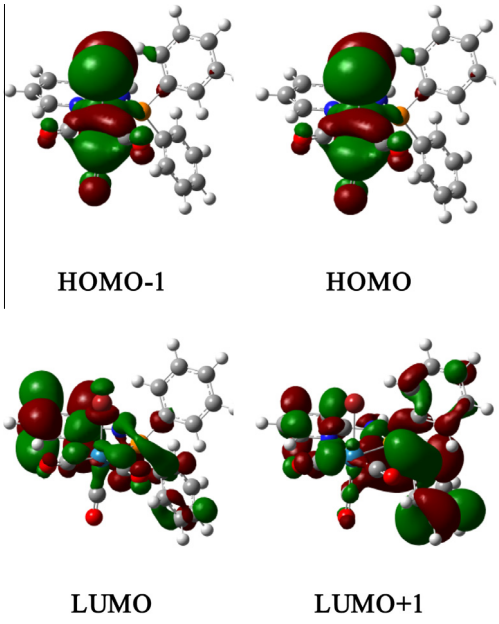

Fig. 6. DFT computed frontier orbitals HOMO−1, HOMO, LUMO and LUMO+1 plots for **RePNN**. A complete set can be found in electronic supplementary information.

occurs after optimization (Table S1), which is consistent with the observed irreversibility of both waves.

3.3. Absorption and emission properties

The absorption spectrum of the **RePNN** complex (Fig. 4a) shows a band centered at 300 nm ($\varepsilon = 6 \times 10^3\ M^{-1}\ cm^{-1}$) with a shoulder at 350 nm ($\varepsilon = 1 \times 10^3\ M^{-1}\ cm^{-1}$). Almost no solvent effect can be observed in the spectra of the complex in solvents of different polarity (DCM or DMF, Fig. 4a). The absorption spectra of the **PNN** ligand in the same solvents were also included for the purpose of comparison. The **PNN** ligand has absorption bands with maxima at 230 nm and 295 nm. The comparison of the spectra of both species allows to assign the higher energy band of the complex to a transition centered on the ligand ($\pi \rightarrow \pi^*$), while the absorption at lower energy could be assigned to a metal to ligand charge transfer transition (MLCT). Upon excitation at 300 nm at room temperature, air equilibrated solutions emit light with a maximum at 365 nm in DCM and at 350 nm in DMF (Fig. 4b). The small Stokes Shift observed is compatible with a $\pi \rightarrow \pi^*$ transition, process which does not have important differences in the geometry of the ground and excited states (similar dipole moment). The emission spectra of the ligand exhibit a similar maximum after excitation at 300 nm, however, as can be seen in Table 2, emission quantum yield values are an order of magnitude higher compared to those for the complex. In both cases, the luminescence is not quenched by oxygen in solution. Excitation spectra at the emission maxima (365 nm) show a band centered at 300 nm, which means that the involved transition corresponds to the ligand orbitals ($\pi \rightarrow \pi^*$) (Fig. S1). The existence of overlap of the wavelengths involved in the absorption and the emission processes, allow the occurrence of the phenomena of light reabsorption. The low concentration of the compounds at each experience and the analysis of its concentration dependency, permit us to be sure that this phenomenon is negligible in our experimental conditions.

At low temperature (77 K), the emission bands for both, the complex and ligand, become clearly structured (Inset on Fig. 4b) which is consistent with a transition centered on the ligand orbitals. For the ligand, an additional shoulder can be observed at

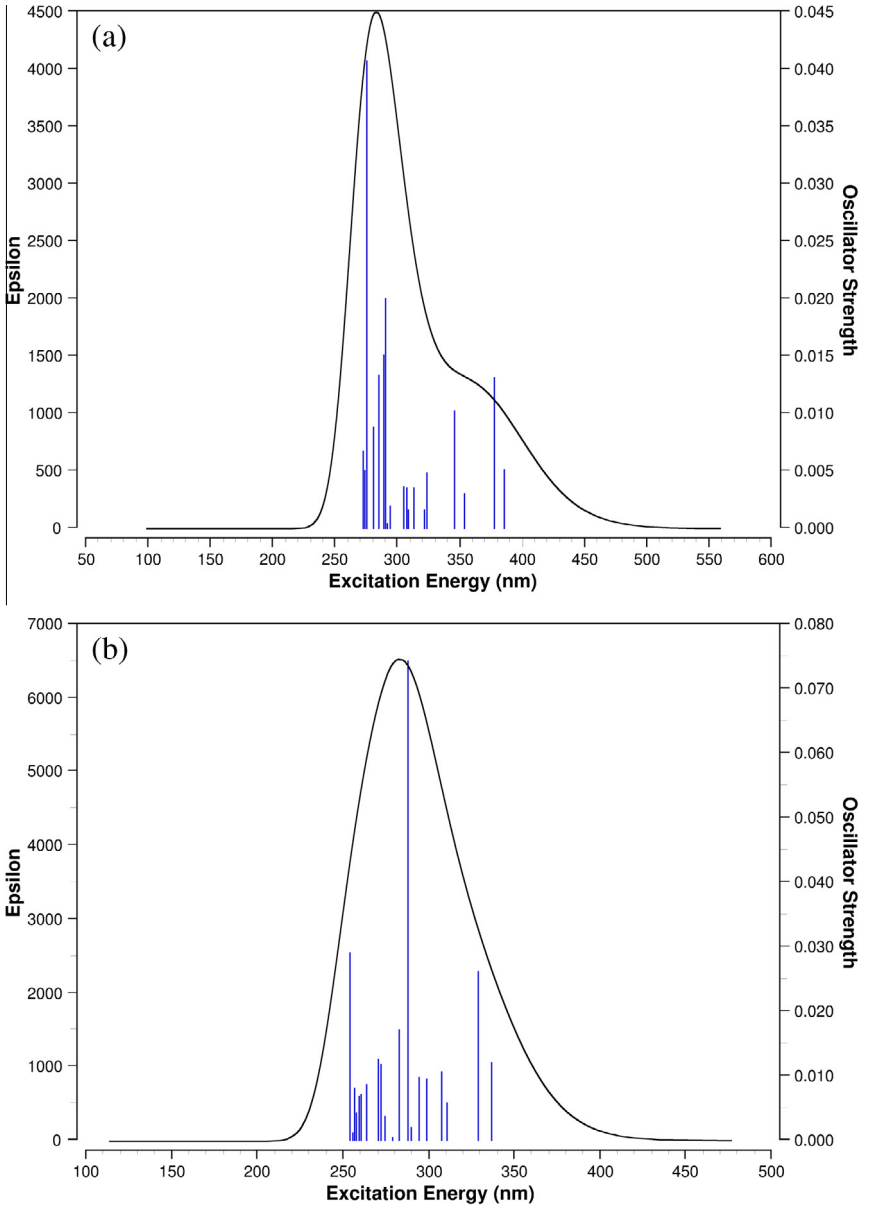

Fig. 7. TD-DFT computed transitions for **RePNN** in gas phase (**a**) and using PCM corresponding to dichloromethane (**b**).

460 nm. The two maxima and the shoulder of the emission spectra would be attributed to a vibrational progression or to the existence of two or more non-equilibrated emissive excited states. Interestingly, we did not appreciate any emission upon excitation at 350 nm either for ligand or complex solutions at room or low temperature.

After pulsed excitation at 300 nm with a delay of 50 μs, a broad and structured phosphorescence emission spectra can be observed for both, the complex and ligand with a maximum around 500 nm and a lifetime of 250 μs (Fig. 4c). Despite the similar shape of both emission bands, the intensity goes strongly down for the complex when compared to the ligand (Fig. 4c inset). These results indicate that the emission processes is related to ligand orbitals, being the MLCT excited state, a sort of quencher of the ligand $\pi\pi^*$ triplet excited state. A fast rate of internal conversion or intersystem crossing processes can happen when two excited states close in energy (and in geometry) are involved. In addition, the presence of a third row metal like rhenium makes the intersystem crossing a favored path [25]. The MLCT excited state is likely to be a non-emissive state, so we did not observe any emission at lower energies. The difference between the band shapes of complex compared with ligand, can be explained in terms of a distortion of the ligand orbital geometry due to the metal coordination [26].

Time resolved experiments for the **RePNN** complex allow us to observe a biexponential luminescent decay at 360 nm after excitation at 280 nm in DCM and DMF solutions (Fig. 5). Lifetimes in the order of a few nanoseconds are measured in both solvents (see Table 2). The amplitude for the long (τ_1) and short (τ_2) components shows a slight dependence with the solvent. Emission decay of the **PNN** ligand in DCM solution shows similar lifetimes but different amplitude values, while in DMF, ligand emission decay has a monoexponential behavior with lifetime of 5.15 ns. These results evidence the presence of two emissive excited states. Moreover, the time-resolved emission spectrum (TRES) of the complex in DCM solution shows the presence of two emission bands very close in energy (inset Fig. 5). The shorter lifetime can be associated with the band centered at 350 nm while the longer one has a maximum at 360 nm. Both, the energies and the lifetimes, can be related to excited states involving the ligand orbitals. In previous studies the biexponential decay of **RePN** complex was related to the presence of two different MLCT triplet excited states very close in energy, one of those involving the pyridine orbitals ($d \rightarrow \pi^*_{py}$) and the other one, the phenyl ones ($d_\pi \rightarrow \pi^*_{ph}$) [14].

Additional evidence supporting the presence of a triplet excited state is based on the detection of singlet oxygen phosphorescence emission upon excitation of complex at 355 nm in DCM solution. A singlet oxygen generation quantum yield of 1.5×10^{-3} was determined, value very close to our limit of detection.

3.4. Computational calculations

In order to get deeper insight of the photophysical behavior of this system, we performed TD-DFT calculation in gas phase and in DCM. Main results are summarized in Table S3. Fig. 6 depicts the DFT computed frontier orbitals HOMO−1, HOMO, LUMO and LUMO+1 plots for **RePNN**. These results support that the lowest energy transition involve a charge transfer from the metal to the pyridine orbitals (MLCT), while the higher energy transitions involve ligand orbitals (complete DFT computed frontier orbitals can be found in supplementary information, Table S1 and Fig. S2). As clear from the comparison between the results for gas phase and DCM, the solvent has a stabilizing effect which results in the shifting to a higher energy of the HOMO–LUMO transition. The simulated spectra shown in Fig. 7, matches well with the experimental results. For comparison, DFT frontier orbitals for the ligand were also computed (Table S2 and Fig. S3). The calculations show that the lower energy bands imply transitions from the pyridine orbitals to phenyl ones ($\pi_{py} \rightarrow \pi^*_{ph}$) and from pyridine to pyridine ($\pi_{py} \rightarrow \pi^*_{py}$). Thus, it is possible to relate the biexponential decay observed for ligand in DCM solution to the co-existence of these two emissive excited states. The slight red-shift of the emission band at low temperature would support this conclusion because these transitions involve minor redistribution of electron density.

Probably, solvent-specific interactions can occur in the case of DMF ligand solution, which would favor the existence of one of these excited states, specifically the $\pi_{py} \rightarrow \pi^*_{ph}$ with longer lifetime. As the lifetimes for the complex are similar, it might be supposed that the observed emission is due to transitions involving the ligand orbitals.

The quenching of the luminescence for the complex can be explained in terms of a fast internal conversion of the $\pi_{py} \rightarrow \pi^*_{ph}$ and $\pi_{py} \rightarrow \pi^*_{py}$ excited state to the non-emissive MLCT excited state. This would be in agreement with the low emission quantum

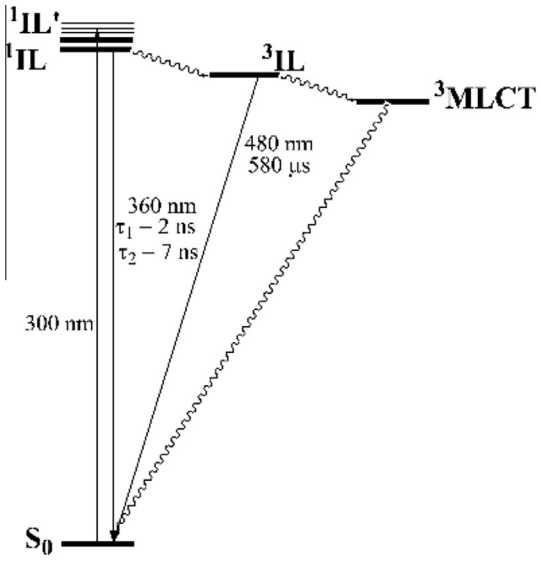

Scheme 3. Schematic energy diagram proposed for all the possible deactivation pathways upon excitation of **RePNN**.

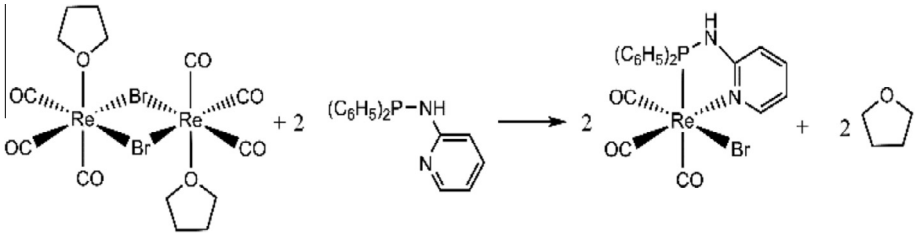

Scheme 2. Synthesis of **RePNN**.

yield observed for the related **RePN** complex, which was explained in terms of the conformational flexibility conferred by the 2-pyridylphosphine ligand [14].

An energy levels diagram is proposed in Scheme 3. As the presence of oxygen does not reduce the emission quantum yields or quenches the lifetimes of ligand or complex, we attribute a singlet character to the ligand $\pi\pi^*$ excited states (^{1}IL and ^{1}IL′ in Scheme 2). These states could evolve to a triplet $\pi\pi^*$ excited states (^{3}IL) or to a non-emissive triplet MLCT excited state (^{3}MLCT), which has been reported to be the more favored excited state for rhenium complexes due to the fast intersystem crossing that singlet excited state undergo as a result of spin-orbit coupling effects [27].

4. Conclusions

The increased flexibility of the ligand 2-(diphenylphosphinoamino)pyridine, **PNN**, when compared to the more rigid **PN**, (due to the presence of NH– fragment between the phosphorous and the pyridyl), enhances the non-radiative decay rate constant from the triplet MLCT excited state to the ground state. The presence of this NH-bridge allows some additional vibration modes that would be coupled to electronic states making the non-radiative path the favored one. Emission of **RePNN** complex comes from ligand centered excited states, being its quantum yield lower than ligand alone due to a favored intersystem crossing to a non-emissive triplet MLCT excited state.

Acknowledgements

The authors gratefully acknowledge financial support of Comisión Nacional de Ciencia y Tecnología, grants FONDECYT 1120865, 1120149 and ACE-03.

Appendix A. Supplementary data

CCDC 1407598 contains the supplementary crystallographic data for [*P,N*-{$(C_6H_5)_2(C_5H_4N)NHP$}$Re(CO)_3Br]\cdot CHCl_3$. These data can be obtained free of charge via http://www.ccdc.cam.ac.uk/conts/retrieving.html, or from the Cambridge Crystallographic Data Centre, 12 Union Road, Cambridge CB2 1EZ, UK; fax: (+44) 1223-336-033; or e-mail: deposit@ccdc.cam.ac.uk. Experimental and computed bond distances for the [*P,N*-{$(C_6H_5)_2(C_5H_4N)NHP$}$Re(CO)_3Br]^+$ cation and the [*P,N*-{$(C_6H_5)_2(C_5H_4N)NHP$}$Re(CO)_3Br]^-$ anion. DFT-computed orbitals for PNN and TDDFT transitions. Supplementary data associated with this article can be found, in the online version, at http://dx.doi.org/10.1016/j.poly.2016.03.014.

References

[1] P. Braunstein, Functional ligands and complexes for new structures, homogeneous catalysts and nanomaterials, J. Organomet. Chem. 689 (2004) 3953.
[2] P. Braunstein, F. Naud, Hemilability of hybrid ligands and the coordination chemistry of oxazoline-based systems, Angew. Chem. Int. Ed. 40 (2001) 680.
[3] P. Espinet, K. Soulantica, Phosphine-pyridyl and related ligands in synthesis and catalysis, Coord. Chem. Rev. 193–195 (1999) 499.
[4] P.J. Guiry, C.P. Saunders, The development of bidentate P, N ligands for asymmetric catalysis, Adv. Synth. Catal. 346 (2004) 497.
[5] G. Helmchen, A. Pfaltz, Phosphinooxazolines A new class of versatile, modular P, N-ligands for asymmetric catalysis, Acc. Chem. Res. 33 (2000) 336.
[6] G.R. Newkome, Pyridylphosphines, Chem. Rev. 93 (1993) 2067.
[7] A. Pfaltz, W.J. Drury, Design of chiral ligands for asymmetric catalysis: from C2-symmetric P, P- and N, N-ligands to sterically and electronically nonsymmetrical P, N-ligands, Proc. Natl. Acad. Sci. U.S.A. 101 (2004) 5723.
[8] B. Machura, R. Kruszynski, Synthesis, crystal, molecular and electronic structure of the [Re(NO)Cl2(PPh3)(PPh2py-P, N)] complex, Polyhedron 25 (2006) 1985.
[9] B. Machura, A. Jankowska, R. Kruszynski, J. Kłak, J. Mroziński, Structural and spectroscopic studies on rhenium(III) diphenyl(2-pyridyl)phosphine oxide complexes, Polyhedron 25 (2006) 2663.
[10] B. Machura, R. Kruszynski, Synthesis, crystal, molecular and electronic structure of the [Re(NO) 0.87Br 2.13(PPh 3)(PPh 2py-P, N)] complex and DFT calculations of [Re(NO)Br 2(PPh 3)(PPh 2py- P, N)], J. Mol. Struct. 837 (2007) 92.
[11] F. Venegas, N. Pizarro, A. Vega, Structural and photophysical properties of a mononuclear Re(I) complex:[P, N-{(C6H5)2(C5H5N)P}Re(CO)3Br], J. Chil. Chem. Soc. 56 (2011) 823.
[12] L. Wallace, D.P. Rillema, Photophysical properties of rhenium(I) tricarbonyl complexes containing alkyl- and aryl-substituted phenanthrolines as ligands, Inorg. Chem. 32 (1993) 3836.
[13] O.S. Wenger, L.M. Henling, M.W. Day, J.R. Winkler, H.B. Gray, Photoswitchable luminescence of Rhenium(I) tricarbonyl diimines, Inorg. Chem. 43 (2004) 2043.
[14] N. Pizarro, M. Duque, E. Chamorro, S. Nonell, J. Manzur, J.R. de la Fuente, G. Gunther, M. Cepeda-Plaza, A. Vega, Dual emission of a novel (P, N) Re(I) complex: a computational and experimental study on [P, N-{(C6H5)2(C5H4N)P}Re(CO)3Br], J. Phys. Chem. A 119 (2015) 3929.
[15] B. Aranda, P. Aguirre, S.A. Moya, M. Bonneau, J.A.G. Williams, L. Toupet, M. Escadeillas, H. Le Bozec, V. Guerchais, Luminescent bis-cyclometallated iridium(III) complexes containing phosphine-based ligands: influence of the P^N bridge, Polyhedron 86 (2015) 120.
[16] M. SAINTPLUS V6.22 Bruker AXS Inc., WI, USA., in.
[17] G.M.S.N.V. Sheldrick, Bruker AXS Inc., Madison, WI, USA, 2000, in.
[18] W. SADABS V2.05 Bruker AXS Inc., Madison, USA., in.
[19] G.A. Crosby, J.N. Demas, Measurement of photoluminescence quantum yields. Review, J. Phys. Chem. 75 (1971) 991.
[20] M.J.T. Frisch, G.W. Schlegel, H.B. Scuseria, G.E. Robb, M.A. Cheeseman, J.R. Scalmani, G. Barone, V. Mennucci, B. Petersson, G.A. Nakatsuji, H. Caricato, M. Li, X. Hratchian, H.P. Izmaylov, A.F. Bloino, J. Zheng, G. Sonnenberg, J.L. Hada, M. Ehara, M. Toyota, K. Fukuda, R. Hasegawa, J. Ishida, M. Nakajima, T. Honda, Y. Kitao, O. Nakai, H. Vreven, T. Montgomery, J.A., Jr. Peralta, J.E. Ogliaro, F. Bearpark, M. Heyd, J.J. Brothers, E. Kudin, K.N. Staroverov, V.N. Kobayashi, R. Normand, J. Raghavachari, K. Rendell, A. Burant, J.C. Iyengar, S.S. Tomasi, J. Cossi, M. Rega, N. Millam, N.J. Klene, M. Knox, J.E. Cross, J.B. Bakken, V. Adamo, C. Jaramillo, J. Gomperts, R. Stratmann, R.E. Yazyev, O. Austin, A.J. Cammi, R. Pomelli, C. Ochterski, J.W. Martin, R.L. Morokuma, K. Zakrzewski, V.G. Voth, G. A. Salvador, P. Dannenberg, J.J. Dapprich, S. Daniels, A.D. Farkas, Ö. Foresman, J. B. Ortiz, J.V. Cioslowski, J. Fox, D.J., Gaussian 09, in, Gaussian Inc, Wallingford CT, 2009.
[21] S. Miertuš, E. Scrocco, J. Tomasi, Electrostatic interaction of a solute with a continuum. A direct utilization of AB initio molecular potentials for the prevision of solvent effects, Chem. Phys. 55 (1981) 117.
[22] S. Miertus~, J. Tomasi, Approximate evaluations of the electrostatic free energy and internal energy changes in solution processes, Chem. Phys. 65 (1982) 239.
[23] W. Humphrey, A. Dalke, K. Schulten, VMD: visual molecular dynamics, J. Mol. Graph. 14 (1996) 33.
[24] Persistence of Vision Pty. Ltd., Persistence of Vision Raytracer (Version 3.6) [Computer software], 2004. Retrieved from http://www.povray.org/download/.
[25] G. Knör, A. Strasser, Coexisting intraligand fluorescence and phosphorescence of hafnium(IV) and thorium(IV) porphyrin complexes in solution, Inorg. Chem. Commun. 5 (2002) 993.
[26] T. Ohno, S. Kato, Ligand–Ligand Interaction in [Zn(1,10-phenanthroline)$_2$(H_2O)$_2$](NO_3)$_2$ and [Zn(2,2′-bipyridyl)$_3$](NO_3)$_2$, Bull. Chem. Soc. Jpn. 47 (1974) 2953.
[27] A. Cannizzo, A.M. Blanco-Rodríguez, A. El Nahhas, J. Šebera, S. Záliš, J.A. Vlček, M. Chergui, Femtosecond fluorescence and intersystem crossing in Rhenium(I) carbonyl−bipyridine complexes, J. Am. Chem. Soc. 130 (2008) 8967.